Characterization of the rear wake of a SUV with extensions and without extensions

Downloaded from: https://research.chalmers.se, 2026-11-14 20:41 UTC

Citation for the original published paper (version of record):
Sebben, S., Sterken, L., Wölken, T. (2017). Characterization of the rear wake of a SUV with extensions and without extensions. Proceedings of the Institution of Mechanical Engineers, Part D: Journal of Automobile Engineering, 231(9 (SI)): 1294-1302.
http://dx.doi.org/10.1177/0954407016678016

N.B. When citing this work, cite the original published paper.

research.chalmers.se offers the possibility of retrieving research publications produced at Chalmers University of Technology. It covers all kind of research output: articles, dissertations, conference papers, reports etc. since 2004. research.chalmers.se is administrated and maintained by Chalmers Library

(article starts on next page)

Characterization of the rear wake of an SUV with and without extensions

Simone Sebben[1], Lennert Sterken[2] and Thies Wölken[2]
[1] Applied Mechanics, Chalmers University of Technology, Sweden
[2] Volvo Car Corporation, Sweden
Corresponding author:
Simone Sebben, Applied Mechanics, Chalmers University of Technology, Hörsalsvägen 7A, Gothenburg, 41296, Sweden
Email: simone.sebben@chalmers.se

Abstract
Passenger vehicles are considered to be bluff bodies and therefore their total aerodynamic resistance is dominated by pressure drag, which is basically the difference between the stagnation pressure in the front and the pressure at the base. In particular, the base wake of a vehicle has a significant influence on the total drag and ways to reduce it and controlling it have been the subject of numerous investigations. The present work focuses on the identification and analysis of unsteady flow structures acting on the base wake of an SUV with and without rear-end extensions. Tapered extensions have proven to be an effective way to reduce drag since they act as a truncated boat-tailing device improving the pressure recovery zone and reducing the wake size. In this investigation, wind tunnel experiments and Computational Fluid Dynamics **were** used to study the forces acting on the vehicle and the un-stationary behaviour of the rear wake flow. For the analysis of the unsteady base pressures, a data structure sensitive filtering approach based on Empirical Mode Decomposition in combination with Fast Fourier Transform and Proper Orthogonal Decomposition were used. The numerical and the experimental results are a good complement to each other and both revealed an antisymmetric mode in the transverse plane related to a flapping of the wake at a Strouhal number around 0.23. Furthermore, a pumping effect, which is a main contributor to the drag, was observed at Strouhal values between 0.04 and 0.07. This is in good agreement with results from research on more simplified model shapes. The rear extensions proved to be a productive way to reduce the drag coefficient and the magnitude of the wake flapping for the yaw angles investigated.

Keywords
Drag reduction, wake, flapping, pumping effect, unsteady flow structures, tapered extensions

Introduction
Consumer demands and governmental legislation for a sustainable society are driving car manufactures to invest significant resources on the aerodynamic development of new vehicles with the objective of minimizing fuel consumption and reducing emissions. Increasing environmental consciousness among customers and manufactures leads the automotive industry to strive for highly optimized designs and energy efficient vehicles. This is seen as a necessity in order to stay competitive in a market that is globalized and volatile. One important contributor to

the total driving resistance, which is then directly related to fuel efficiency, is the aerodynamic drag of the vehicle. The aerodynamic drag of a passenger vehicle is basically governed by the pressure difference between the forward and rearwards facing surfaces. Ways to minimize this difference using techniques that reduce the wake size and particularly aim to increase the base pressure by stabilizing the unsteady nature of the rear wake are a matter of continuous research. A well-known method for achieving such results is the use of tapered extensions attached to the rear end of the car. The extensions create a cavity and can also be interpreted as creating a boat-tailing effect. A thorough overview of drag reduction devices for the base area are extensively described in References [1-5]. Specifically, the effects of base-cavity, base bleed, active blowing and splitter plate techniques are discussed in References [3-8]. Recent work on a full-size SUV with attached rear-end extensions was conducted both experimentally and numerically in [9-10]. The results of the study successfully showed that the technique of tapered extensions works well even at relatively large yaw angles and that it is possible to achieve drag reduction while still maintaining vehicle stability. This was principally achieved with the use of a so-called kicker, a small device attached to the edge of the extensions with the objective of reducing the lateral- and normal-velocity components in favour of the longitudinal component upon flow separation.
The present work focuses on the identification and analysis of unsteady flow structures acting on the base wake of an SUV with and without rear-end extensions at different yaw angles. The work was conducted both experimentally and numerically, and the results obtained complement each other regarding forces, unsteady base surface pressure and frequency of flow field fluctuations. Experimentally, the force analysis and the study of the unsteady wake behaviour were conducted in different campaigns. Previous research [11] on unsteady effects of the base wake behind a simple square back model showed that the principal contributor to the aerodynamic drag can be associated to a pumping effect of the wake with a frequency corresponding to 0.8 to 1 Hz, equivalent to a Strouhal number, Sr, of approximately 0.04. A comprehensive analysis of the turbulent wake structure behind an Ahmed body, its global modes and bi-stable behaviour with coupling to base pressure and drag is well explained in the work of Grandemange et al. [12,13]. Additional discussions of the near-wake nature can be found in the work of Sims-Williams [14], for example. In search of observations of similar behaviour, unsteady base pressures measurements were conducted experimentally. This allowed for a correlation between different assessment locations that helped to bring insight on the flow structures behind the model. The high temporal resolution and duration of the experimental samples enabled the low frequencies relevant to wake modes to be captured, but spatial resolution was insufficient, as the number of sensors was limited. Therefore, a technique based on Empirical Mode Decomposition (EMD) was used, where the signal was decomposed in multiple modes ordered from high to low frequencies. This allowed for a signal reconstruction with the modes in the desired frequency range.
Computational Fluid Dynamics (CFD) results enrich the experimental analysis by bridging the shortcoming in spatial resolution of the surface pressures and by giving more insight into the flow field. The CFD analysis allowed for the correlation of several wake planes which was a limitation in the measurements performed in the wind tunnel.

Methodology

This section gives a description of the test object and the experimental and numerical setup. It also provides a short explanation of the techniques used for acquiring the modes and frequencies.

Test object

The results presented in this paper are retrieved from the analysis on a modified Volvo XC60 AWD that includes additional underbody panels, a covering of the stop lamp feature at the roof, and a closed upper and lower grille. This is considered as the baseline configuration. The modifications were added in order to guarantee a good flow quality entering the base wake which is a pre-requisite for a good performance of the extensions. The vehicle exterior and the underbody with the mounted panels is seen in Figure 1.

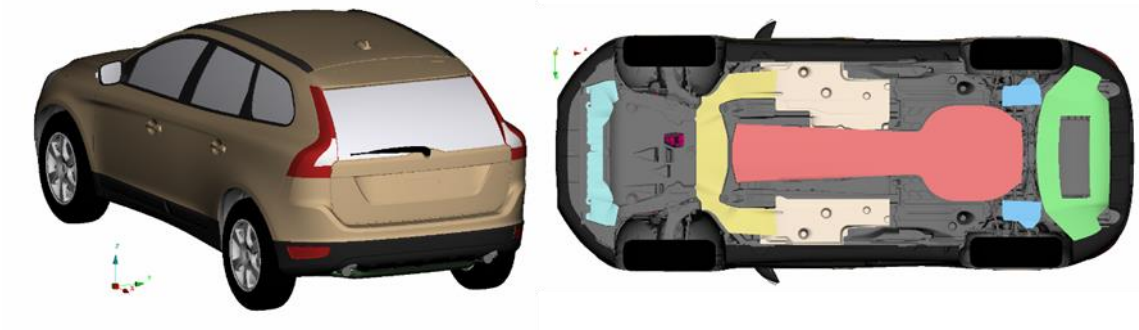

(a) (b)

Figure 1. Test object: (a) **rear**-side view, and (b) improved underbody with mounted panels.

As discussed previously, several investigations [5,9,15] show the benefit of tapered rear-end extensions to alter the base wake with the intension of reducing the aerodynamic resistance. Here, an extended analysis of the effect of the extensions used in [15] was performed with a focus on the response of the flow unsteadiness in the wake. In particular, the extensions with a length of 0.15 m were chosen and installed in the baseline model at their most effective angle. A sketch of the extension profile with the kicker at the symmetry plane is seen in Figure 2. The concept behind the addition of the extensions and the kicker is based on the equation for the local drag which is discussed next.

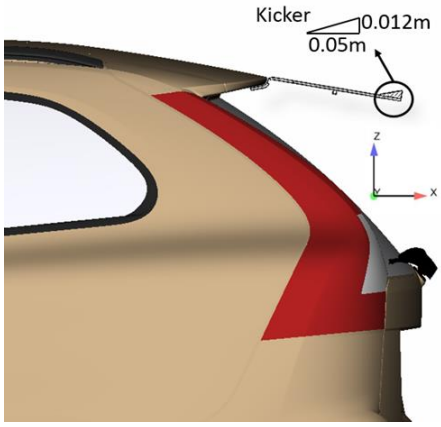

Figure 2. A sketch of the extensions and the kicker at the symmetry plane.

Local drag

An informative way to visualize and quantify wake losses is by using the notion of local drag which is defined by Cogotti [16] according to equation (1). The expression represents losses due to the total-pressure (*Term I*), longitudinal kinetic energy (*Term II*) and vorticity (*Term III*).

$$CdA = \underbrace{\int_{S_{Wake}} \left(1 - c_{p_{tot}}\right) dS}_{\textit{Term I}} - \underbrace{\int_{S_{Wake}} \left(1 - \frac{V_x}{V_\infty}\right)^2 dS}_{\textit{Term II}} + \underbrace{\int_{S_{Wake}} \left(\frac{V_y^2 + V_z^2}{V_\infty^2}\right) dS}_{\textit{Term III}} \quad (1)$$

According to the equation, *Terms I* and *III* add to drag and their values should be minimized, while *Term II* has always a negative contribution. The inclusion of tapered extensions reduces the rear wake size, *dS*, which improves drag in general. It also reduces *Term I* in equation (1) due to the increase of the base pressure of the model. The kicker contributes to the reduction of *Term III* by minimizing the lateral- and normal-velocity components. It is to be noted however, that the addition of the kicker results on a slightly larger rear wake when compared to the configuration with the **extensions only. This** causes an increase in drag which can annul the reduction obtained in *Term III* in some situations.
The magnitude of the third term, also called vortex drag is visualized in Figure 3 at a plane 0.1 m behind the vehicle for yaw = 0.

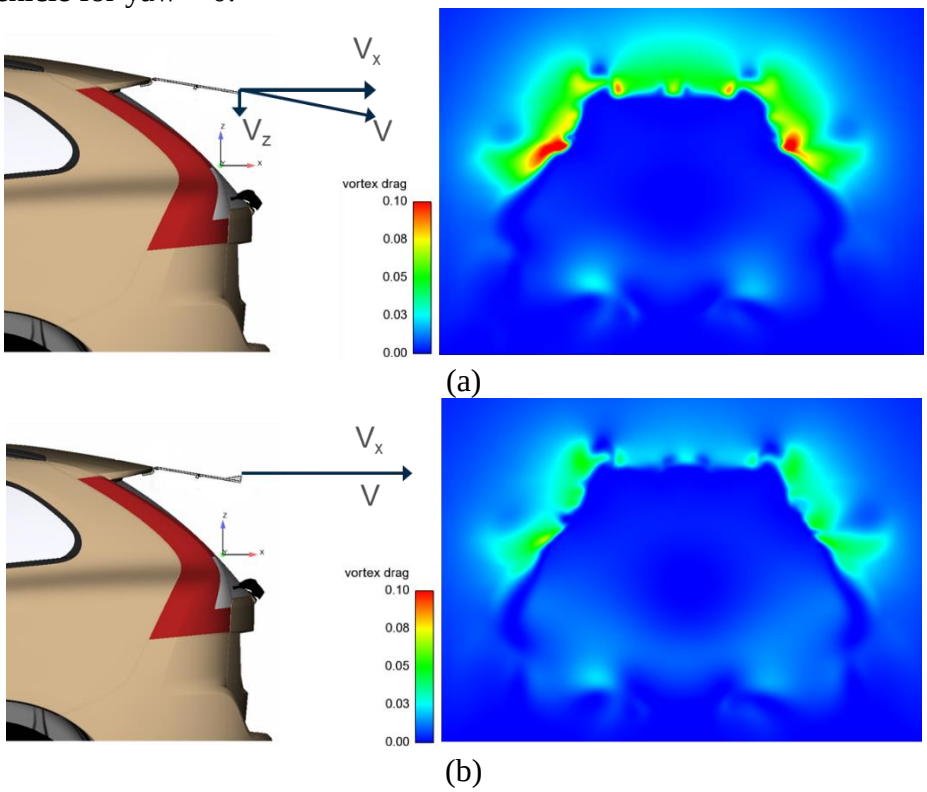

Figure 3. Visualization of vortex drag, *Term III* in equation (1) for: (a) configuration with extensions, and (b) configuration with extensions and kicker.

Experimental set-up

All experimental measurements were conducted in the full-scale Volvo Cars Aerodynamic Wind Tunnel (PVT) and at a speed of 100 kph. The tunnel is of a Göttingen type with a slotted-wall test section and a cross-sectional area of 27 m^2. In order to simulate real road flow conditions around a vehicle, a boundary layer control system (BLCS) is available. The system contains a scoop at the start of the test section, a boundary-layer suction area, a five-belt moving-ground system, and tangential blowing behind each of the five belts [17]. It ensures an uncertainty of less than 0.001

for Cd and Cl_F and less than 0.003 for Cl_R for measurements within the same test. The tunnel is accredited according to the European Accreditation procedure EA 4/02.
For the study of the periodic base wake structures, an initial evaluation of the empty wind tunnel was conducted in order to check that neither the wind tunnel fan nor the boundary layer control system produced periodic variations that could affect the wake pressure measurements when the car was present in the test section. For this, the pressure sensors were mounted in poles which were spread over the width of the test section and were movable. Care was taken so that the measurement signals were not distorted by the interference of the flow with the poles. Sensors from First Sensors of the HCLA-type were positioned at the inside of the surface shell with 0.05m-tubing leading to the measurement location. Their range is ±2500 Pa with a static calibration to an accuracy of ±5 Pa which for the flow regime investigated, allows for an accuracy in the coefficient of pressure, C_p, equivalent to 0.01 at 100 kph. Results of the spectral response of the wind tunnel systems indicated that periodic variations from the fan, moving ground and BLCS were not significant and could be neglected in this investigation. Low-frequencies originated from other parts of the tunnel circuit were not investigated as their contribution was assumed to be smaller than the fan and BLCS system.
For the vehicle measurements, unsteady surface pressures were assessed near the base perimeter where separation is expected to occur in order to capture the strongest flow fluctuations. In the reference configuration (without extensions), 14 pressure-sensors were mounted on the inside of the vehicle surface shell with a 0.05 m tube leading to the measurement location. Most of the sensors were positioned in the rear-lamp region where the flow is expected to show a strong unsteady behaviour. Two additional sensors were placed at the symmetry line, see Figure 4.

Figure 4. Locations of the unsteady pressure sensors mounted on the base perimeter.

Signal processing

The raw signal obtained by the unsteady pressure sensors over time is complex and difficult to interpret. It is hidden under a broad spectrum of fluctuations and noise. Therefore it is necessary to analyse the signals to extract spatial and spectral information of the structures related to the global behaviour of the wake.
Fast Fourier Transform (FFT). To analyse its spectral content a signal can be transformed from its time domain to its frequency through the often used Fourier transformation, equation (2). From the FFT the energy contribution of the signal p(t) can be calculated with the Power Spectral Density function (PSD), equation (3).

$$(f) = \int_0^T p(t) e^{-i2\pi f t} dt \qquad (2)$$

$$PSD(f) = \frac{2}{T}|P(f)|^2 \quad (3)$$

Empirical Mode Decomposition (EMD). With EMD a signal is decomposed through a sifting process into Multiple Intrinsic Mode functions (IMF's) sorted based on their frequency content in a descending order. At the end of this process only a residue of the signal remains with temporal trend of the signal. A more detailed explanation of the sifting process and the definition of an IMF can be found in [15]. As these modes are a direct result of the signal itself, the latter can be reconstructed through summation of the modes and residue, see equation (4), or any subset can be chosen with the modes in the frequency range of interest.

$$p(t) = \sum_{j=1}^{n} IMF_j + r_n \quad (4)$$

These modes represent a physical meaning where their frequencies and amplitudes are dependent on time as they adapt to changes in the physical environment. Therefore the EMD can be useful approach for non-stationary and non-linear data analysis [18].

Proper orthogonal decomposition (POD). POD is a multivariate statistical analysis method that can be used to decompose the data into orthogonal uncorrelated modes ranked by the amount of variance in the complete dataset from high to low. This approach can be applied to both the experimental and numerical data to reveal relevant coherent structures. The complete data is united in a matrix X, which can be decomposed into $X = USV^T$. Here the diagonal elements of the matrix S are equal to the square-root of the eigenvalues of $X.X^T$ and the matrix V contains the eigenvectors belonging to each eigenvalue and represents the direction of the principal component. The matrix U is the projection matrix of the data X onto the directions of the principal components.
The POD technique can be implemented as a bi-orthogonal decomposition where it not only provides spatial information for each mode or topos, but also temporal modes, chronos, describing the development of the topos over time. Therefore it can be considered an interesting choice for the analysis of periodic coherent wake structures [19].
All POD results presented here are based on the pressure field, unless otherwise stated.

Numerical set-up

For the CFD simulations, the geometrical CAD-data **resembled** with good accuracy the physical model. Volume meshes of around 170 million cells with five to seven **prism** layers near the surface to give an $y^+ = 20$, were used together with Ansys Fluent as the CFD solver. A rather extensive mesh study was conducted in order to guarantee a relatively independent mesh solution. The numerical simulations were performed with the Delayed Detached Eddy Simulation (DDES) with the Spalart-Allmaras (SA) turbulence model, after an initialization from a steady-state Reynolds averaged k-ε model converged solution. After an initial simulation time, the time step was set to 0.0002 s which results in a CFL number somewhat higher than 1. However, a study conducted with a reduced time step and thus, lower CFL, resulted in negligible changes in the force values. Hence, it was assumed that the time step of 0.0002 s was a good compromise between accuracy and computational costs. The overall running time was over six seconds in order to guarantee a good running average. For each force coefficient the running average started at time t = 2.0 s including an additional safety margin. For a reliable averaged value, about three seconds of integration was required before the force coefficients were sufficiently averaged. With

these settings, rear-lift coefficients agreed quite well with the wind tunnel data and drag values were within 3% in accuracy for all cases studied. More detailed information on the numerical method and its validation is found in [10].
A view of the model in the numerical domain together with a series of planes used for post-processing is depicted in Figure 5.

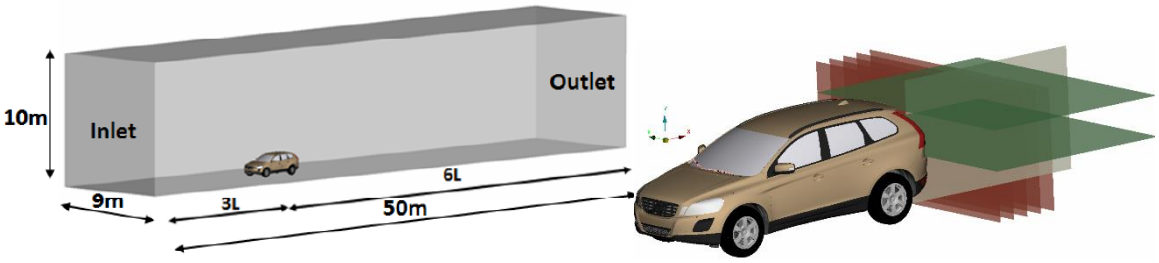

(a) (b)

Figure 5. (a) Vehicle positioning in the numerical wind tunnel, and (b) planes containing the data for the analysis of the numerical results.

Results

Results for global delta drag forces obtained in the wind tunnel and data related to the unsteady surface base pressure measurements are discussed in this section. As mentioned, the high temporal resolution and duration of this data provides a good basis for recovering data over the relevant frequency range. This is partially overcome with results from CFD simulations and POD.

Global drag delta forces

The effect of the tapered extensions and the addition of the kicker on the drag coefficient relative to the reference are summarized in Figure 6. The experimental data is taken from [9] and confirms that drag reduction is obtained with the modifications attached at edge of the base, at small yaw angles. At 0º yaw, a slight increase in drag is observed with the kicker. As explained earlier, the decrease in vortex drag can be overcome by the larger wake size resulting from the addition of the kicker. However, the kicker is still beneficial since it promotes a less sharp increase of the drag coefficient with yaw and it practically doubles the drag reduction under yaw up to ±5º when compared to the extensions only.

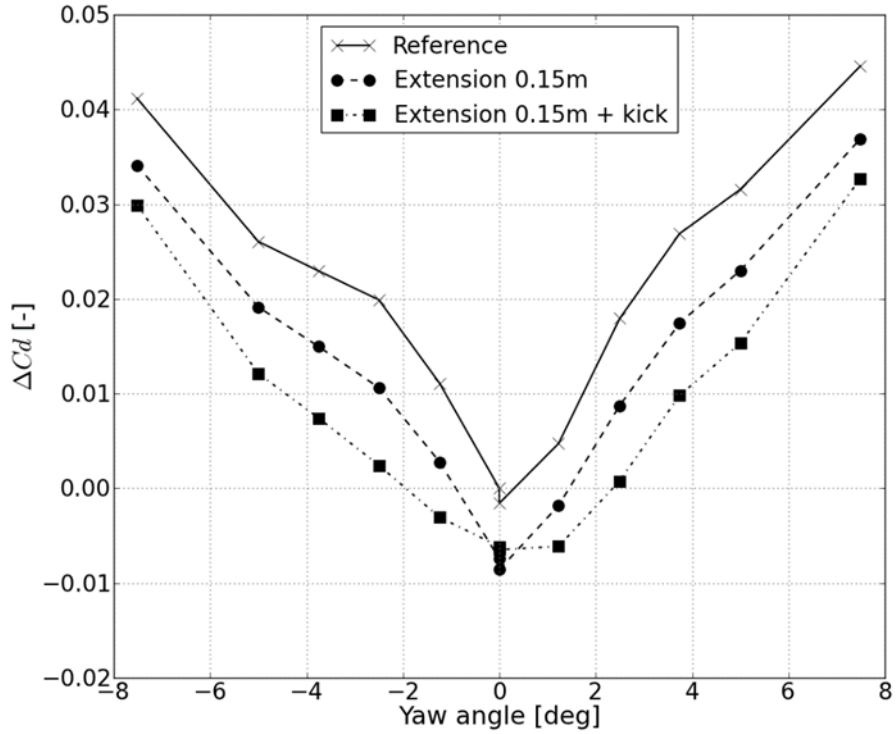

Figure 6. Delta drag coefficient versus yaw angle: Experimental results.

Asymmetric wake behaviour

For the experimental analysis of the wake periodicity a pressure centre movement approach was used to relate the signals from the sensors at the base. The centres, named PC1 and PC2, were calculated from the measurements of the right and left sensors positioned above and below the vehicle catwalk, respectively. The approach was used to identify a flapping motion.

A spectral response of the horizontal fluctuations of the centres of pressure, PC1 and PC2, revealed a periodic pattern with a peak at Sr ~ 0.23 which agrees well with typical Strouhal numbers given in the literature related to an asymmetric flapping motion of the wake or vortex shedding behind bluff bodies. In order to further investigate the data in this frequency interval, the EMD approach was used to filter each signal obtained with the pressure sensors at the base. Only modes containing a significant amount of power spectral density between $0.15 < Sr < 0.3$ were considered. A first impression of the pressure fluctuations and a clear asymmetric behaviour can be seen in Figure 7 (a) and (b) for time steps t = 0.16 s and t = 0.3 s, respectively. At t = 0.16 s the pressure on the left side of the car is close to zero or negative while it is positive in nearly every sensor on the right side. At t = 0.3 s the situation is reversed. Within one second, four full periods of changeover were counted resulting on a Strouhal number around 0.25 which is well within the interval of wake flapping.

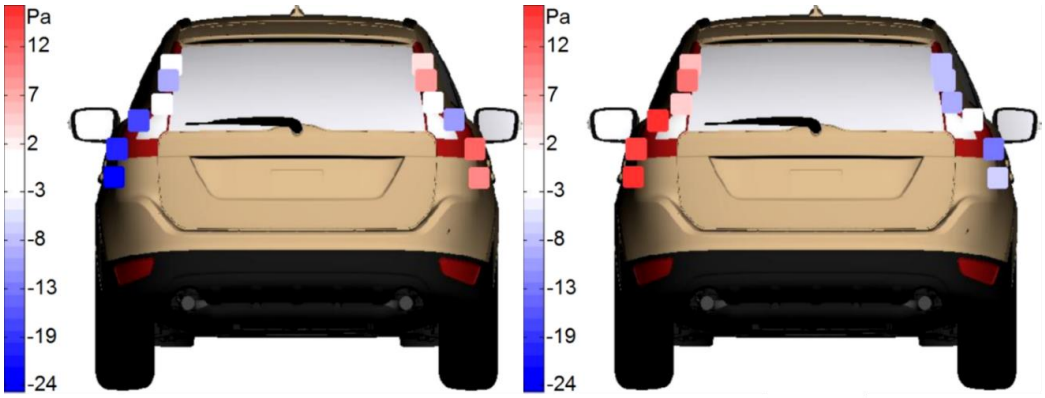

(a) (b)

Figure 7. Distribution of pressure filtered to flapping related interval at: (a) t = 0.16 s, and (b) t = 0.3 s.

By using a combination of POD with EMD on the pressures and by filtering the data set to a desired bandwidth it is possible to obtain the topos of the first mode which show the asymmetric behaviour between the left and right sides. The lower two sensors contribute mainly to the first mode as they measure the strongest overall fluctuations. An anti-correlation between the left and the right sides is seen below the catwalk where the rear end of the vehicle is practically vertical. Even though peaks for flapping can be found in the spectral responses of all sensors, the typical asymmetric bluff body behaviour is strongest at the lower part. The topos and the FFT of the chronos are shown in Figure 8. It is concluded that the POD is a sufficient approach to verify an asymmetric flapping of the wake in the experimental data. Important to notice is that similar observations as the one from Figure 8 can be derived from the measurements at low yaw angles.

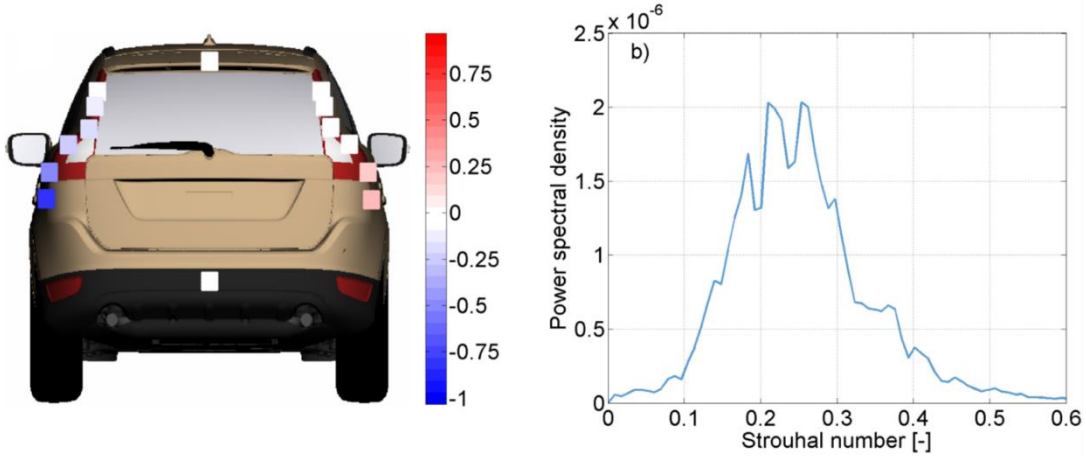

(a) (b)

Figure 8. First POD mode calculated with pressure fluctuations from flapping interval: (a) topos, and (b) FFT of the chronos.

POD can be also applied to the numerical data and an asymmetric flapping mode can be found in modes three and four of the lower transverse plane. Figure 9 shows the topos with grey dots where the time-averaged boundary of the wake is. The topos visualize an asymmetric shedding while the spectral responses of the chronos reveal seven peaks of similar power spectral density. When evaluating the peaks from all modes together, the most dominant one appears at Sr = 0.26. The numerical data does not perfectly match the Sr = 0.23 from the experimental results but

confirms the existence of an antisymmetric wake behaviour and provides a more clear picture of the flow structures involved.

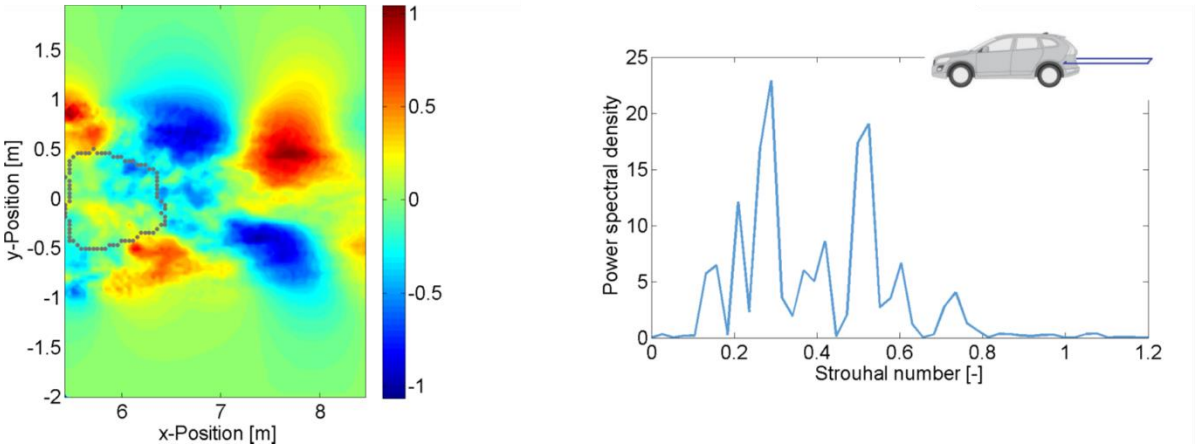

(a) (b)

Figure 9. CFD results of the topos and chronos at lower z-plane: (a) fourth POD mode topos, and (b) FFT of the chronos.

Regarding the results with the rear extensions it is possible to see from the experimental data a reduction of the wake flapping compared to the reference car. This is clear in Figure 10 where the pressure normalised lateral centre position is plotted against time. The graphs are a result of the complete pressure signal, with a super-imposed line based on filtered pressures in the range of 0.5-20 Hz with the EMD-technique.

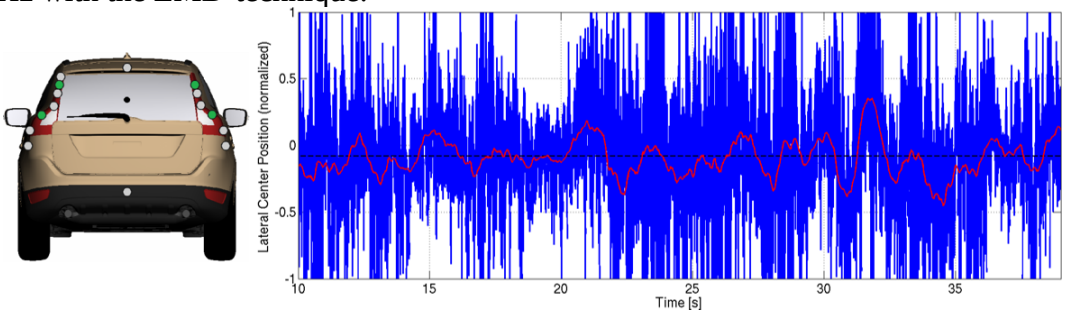

(a)

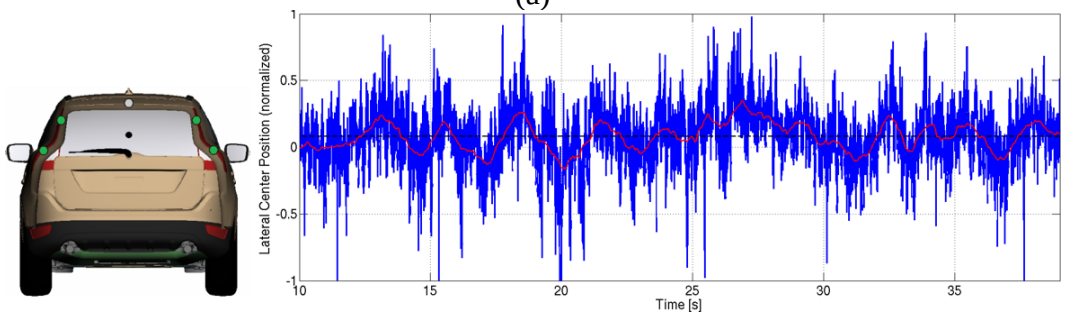

(b)

Figure 10. Lateral pressure centre position: (a) baseline, and (b) vehicle with extensions.

Longitudinal wake movement

Figure 11 shows the third mode resulting from the POD of the experimental data pre-filtered to the interval Sr < 0.1 for the reference car. It contains most of its fluctuation originating from the pumping interval below Sr = 0.1, and all the sensors are positively correlated with the mode.

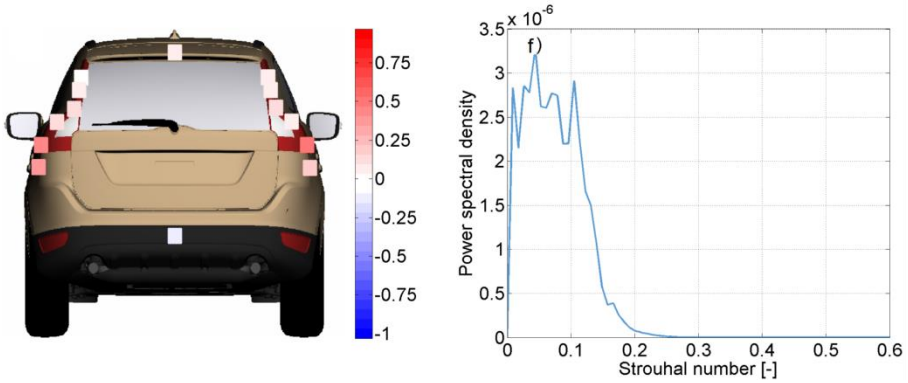

(a) (b)

Figure 11. Third POD mode pre-filtered to Sr < 0.1: (a) topos, and (b) FFT of the chronos.

Results with the extensions are shown in Figure 12 for the second POD mode. It represents pressure fluctuations that are correlated with all sensors symmetrically. The extensions do not change the structure of the flow revealed by the POD modes at these low frequencies.

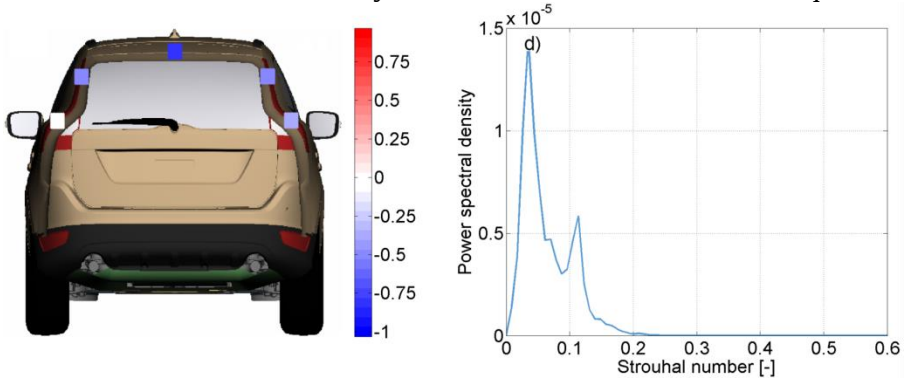

(a) (b)

Figure 12. Third POD mode pre-filtered to Sr < 0.1: (a) topos, and (b) FFT of the chronos.

Looking at the reconstruction of the flow field associated to the first POD mode at the higher z-plane, a symmetric mode with two large counter-rotating vortices 2 m behind the vehicle and a strong longitudinal variance is observed in Figure 13. Such flow structure is associated with the pumping oscillation of the closure region of the near wake. The mode is similar to the symmetric second mode in a horizontal plane behind a square back generic SUV presented in [20]. However the longitudinal variance in the flow field is higher in Figure 13, which adds to the pumping effect.

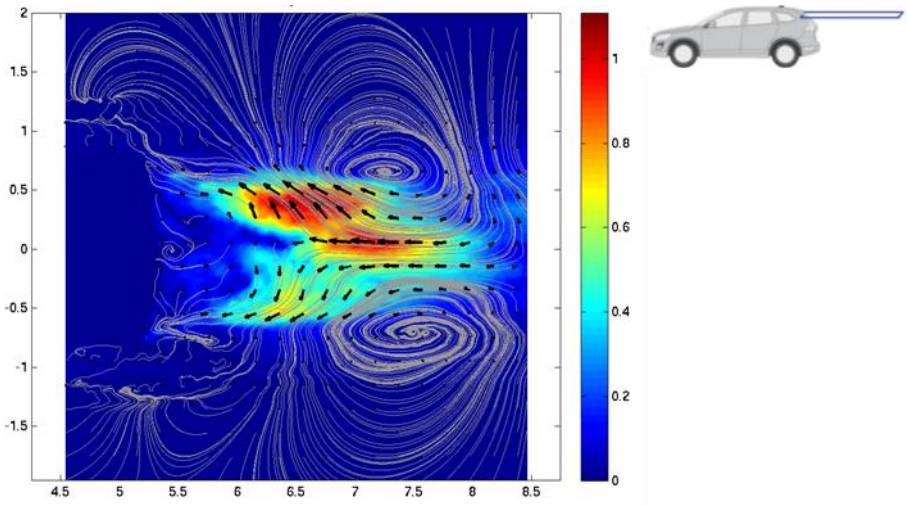

Figure 13. First POD mode in the higher horizontal plane based on the V_x and V_y components.

Conclusions

The base pressure and the rear wake are responsible for a significant amount of the overall drag of a vehicle. In his work, a passive technique was used to control the wake flow with the objective of reducing drag without negatively influencing the rear lift. The technique consisted of tapered extensions with the addition of a so-called kicker. The concept of the kicker originated from the evaluation of the local drag equation and aimed to guide the flow in a parallel direction upon separation, thus minimizing losses due to changes in longitudinal velocity and by reducing the contribution of vortex drag. The approach proved to be successful as drag reductions of as much as 0.010 to 0.020 were obtained. To further understand the validity of the tapered extensions and the kicker, an analysis of the wake periodicity and wake pumping was conducted both experimentally and numerically. Experimentally, unsteady surface pressures sensors were used to obtained information of the flow at the base area. An EMD and POD approach were used to study the data and proved to be a powerful analysis toolbox for the study of non-stationary wakes. Numerical simulations complemented the investigation by revealing more information of the flow. The present results confirmed an antisymmetric mode behaviour in the transverse plane related to a flapping of the wake at Strouhal number around 0.23 which is typical of bluff bodies. Additionally, a pumping effect which is a main contributor to the drag, was observed at Strouhal values between 0.04 and 0.07. The extensions were able to reduce the magnitude of its effect.

Acknowledgments

This work would not have been possible without the support of Volvo Car Corporation and the Swedish Energy Agency (FFI) through the project funding P34537-1.

References

1. Viswanath PR. Flow management techniques for base and afterbody drag deduction. *Progress Aerospace Science* 1996; 32: 79-129.
2. Tanner M. Reduction of base drag. *Progress Aerospace Science* 1975; 16: 369-384.
3. Irving Brown Y, Windsor S and Gaylard A. The effect of base bleed and rear cavities on the drag of an SUV. SAE paper 2010-01-0512, 2010.

4. Howell J, Sims-Williams D, Sprot A, et al. Bluff body drag reduction with ventilated base cavities. *SAE Int J Passenger Cars Mech Syst* 2012; 5: 152-160.
5. Khalighi B, Balkanyi SR and Bernal LP. Experimental investigation of aerodynamic flow over a bluff body in ground proximity with drag reduction devices. *Int J Aerodyn* 2013; 3: 217-233.
6. Gilliéron P and Kourta A. Aerodynamic drag reduction by vertical splitter plates. *Exp Fluids* 2010; 48: 1-16.
7. Littlewood R, Passmore M and Wood D. An investigation into the wake structure of square back vehicles and the effect of structure modi cation on resultant vehicle forces. SAE paper 2011-37-0015, 2011.
8. Littlewood R and Passmore MA. Aerodynamic drag reduction of a simplified squareback vehicle using steady blowing. *Exp Fluids* 2012; 53: 519-529.
9. Sterken L, Lofdahl L, Sebben S, et al. Effect of rear-end extensions on the aerodynamic forces of an SUV. SAE paper 2014-01-0602, 2014.
10. Sterken L, Sebben S and Lofdahl L. Numerical implementation of Detached Eddy Simulation on a passenger vehicle and some experimental correlation. *J Fluids Eng* 2016; 138: 1-14.
11. Duell E and George A. Experimental study of a ground vehicle body unsteady near wake. SAE paper 1999-01-0812, 1999.
12. Grandemange M, Gohlke M and Cadot O. Turbulent wake past a three-dimensional blunt body. Part 1. Global modes and bi-stability. *J Fluid Mech* 2013; 722: 51-84.
13. Grandemange M, Gohlke M and Cadot O. Turbulent wake past a three-dimensional blunt body. Part 2. Experimental sensitivity analysis. *J Fluid Mech* 2014; 752: 439-461.
14. Sims-Williams DB. *Self-excited aerodynamic unsteadiness associated with passenger cars*. PhD Thesis, Durham University, UK, 2001.
15. Sterken L. *Analysis of the unsteady flow field of a passenger vehicle*. PhD Thesis, Chalmers University of Technology, Sweden, 2015.
16. Cogotti A. A strategy for optimum surveys of passenger-car flow fields. SAE paper 890374, 1989.
17. Sternéus J, Walker T and Bender T. Upgrade of the Volvo Cars Aerodynamic Wind Tunnel. SAE paper 2007-01-1043, 2007.
18. Huang NE, Shen Z, Long SR, et al. The Empirical Mode Decomposition and the Hilbert Spectrum for nonlinear and non-stationary time series analysis. *Proceedings of the Royal Society of London A: Mathematical, Physical and Engineering Sciences* 1998; 454. issue 1971.
19. Liang YC, Lee HP, Lim SP, et al. Proper Orthogonal Decomposition and its applications-Part I: Theory. *J Sound Vib* 2002; 252: 527-544.
20. Al-Garni AM, Bernal LP and Khalighi B. Experimental investigation of the flow around a generic SUV. SAE paper 2004-01-0228, 2004.